 doi:10.20944/preprints202202.0193.v1

Article

A Machine Learning Approach for Improved Inertial Navigation System Solution

Ahmed E. Mahdi [1], Ahmed Azouz [1], Ahmed Abdalla [1], and Ashraf Abosekeen[1]*

[1] Electrical Engineering Branch, Military Technical College, Kobry El-Kobba 11766, Cairo, Egypt ; ahmedelgibly@yahoo.com (A. E. M.); a.azouz@mtc.edu.eg (A.A.); elsaid_a@mtc.edu.eg (A.A.)
* Correspondence: a.abosekeen@ieee.org

Abstract: Inertial navigation system (INS) is a basic component for obtaining a continuous navigation solution in various applications. The INS navigation solution suffers from a growing error over time. In particular, its navigation solution depends mainly on the quality and grade of the inertial measuring unit (IMU) that provides the INS with both accelerations and angular rates. However, low-cost small micro-electro-mechanical systems (MEMS) suffer from tremendous error sources such as bias, scale factor, scale factor instability, and highly non-linear noise. Therefore, MEMS-IMU measurements lead to drifted solutions when used as a control input to the INS. Accordingly, several approaches have been introduced to model and mitigate the errors associated with IMU. In this paper, a machine learning-based adaptive neuro-fuzzy inference system (ML-ANFIS) is proposed to leverage the performance of low-grade IMUs in two phases. The first phase is training 50% of the low-grade IMU measurements with a high-end IMU to generate a suitable error model. The second phase involved testing the developed model on the remaining low-grade IMU measurements. A real road trajectory was conducted to evaluate the performance of the proposed algorithm. The results show the effectiveness of utilizing the proposed ML-ANFIS algorithm in removing errors and improving the INS solution compared to the traditional one. An improvement of 70% in the 2D-positioning and 92% in the 2D-velocity INS solution is attained when the proposed algorithm was applied compared to the traditional INS solution.

Keywords: INS, MEMS-IMU, Machine Learning, ANFIS, Positioning, Navigation

1. Introduction

With the advantage of being a self-contained system and providing an uninterrupted navigation solution, the inertial navigation system (INS) has become an essential component for obtaining a robust navigation solution in several applications such as aircraft applications, autonomous navigation, and vehicle dynamic control [1]. However, the advantage of the INS is that it has high short-time accuracy because it suffers from drift accumulation of biases over time. The accuracy of the INS's navigation solution and the ability to reduce the errors accumulated over time depends on the type of inertial measuring unit (IMU) [2]. Lately, the utilization of micro-electro-mechanical systems (MEMS) has been developed for inertial sensor systems with the advantages of low cost, small size, and low power consumption [3]. On the other hand, the MEMS disadvantage of the high error accumulation rate raised the challenge of modeling these errors to improve the accuracy of the navigation solution [4].

The difficulty in modeling these errors was due to the existence of non-linear errors. These errors cannot be modeled by the traditional techniques such as the Kalman filter (KF), the extended KF (EKF), the unscented Kalman filter (UKF), or even by the particle filter (PF) [2,5]. Accordingly, there is a great need to find an alternative to traditional methods that do not require the difficulty and complexity of error modeling. Therefore, the researchers took advantage of the availability of a large amount of data extracted from the INS and inserted the machine learning (ML) techniques in the navigation algorithm [5,7–9].

The ML techniques are utilized as estimators/predictors or classifiers for the navigation parameters. These techniques are utilized in smoothing the choice of applicable sensors as an alternative to KF in a plug-and-play manner [5,7]. This leads to the fleeting

 doi:10.20944/preprints202202.0193.v1

selection of the integration process and raw measurements. Consequently, training the ML model helps in producing a robust predictive model for the INS errors during the GNSS outages. In addition, it can be used in improving visual positioning, mitigating the non-line-of-sight (NLOS) effects such as the multipath effect, spoofing, and jamming [10].

There is a growing interest in utilizing ML techniques in improving the INS navigation solution. An approach utilizing the artificial neural networks (ANN) to overcome the limitations of the KF in bridging the GPS outages during the GPS/INS integration process is introduced in [11–14]. The proposed methodology was accomplished in two phases. In the first phase, the ANN was trained to predict the INS position error and remove it from its corresponding INS position without getting the initial position of the INS system. Furthermore, the work in [15,16] utilized the ANN and ANFIS after the GPS/INS integration to enhance the INS navigation solution. In contrast, the work [17] introduced a non-linear autoregressive neural network with external inputs (NARX) combined with UKF to enhance the position and velocity accuracy of the INS/GNSS integration. Furthermore, the work in [2] proposed a fast orthogonal search (FOS) model to reduce and compensate the unmodeled residual non-linear errors of a Mag/Radar/RISS/GPS integration system to improve the navigation solution during the GPS outages. While the work in [18]utilizes the FOS model as a GPS swept anti-jamming technique to discriminate between the GPS authentic signal and the interference by the chirp frequency jammer. In [19] two approaches were introduced to overcome the drift during GNSS outages using parallel cascaded mechanization for non-linear error estimation of the INS solution. The results show slight improvement during the parts of the trajectory that had maneuvers such as turns, while the low maneuvers parts had a significant improvement. The work in [20] proposed a random forest (RF) method for standstill recognition. The proposed method depends on the generated features from the IMU signals that represent the standstill state as an input for the classifier.

In comparison, the work in [21] introduced a supervised machine learning technique for spoofing detection. The work in [22] introduced an Adaptive Fuzzy Extended Kalman Filter (AFEKF) to enhance the prediction level of the position and velocity errors of the INS. In [5,7] the authors introduced a sensor fusion technique based on fuzzy clustering to fuse between doppler speed from an FMCW radar and speedometer data to improve the input speed to a RISS model. The results show enhancement of the navigation solution in some portions of the trajectory. on the other hand, the lack of sensor fault detection and false reading algorithm causes a drift in some portions which had wheel slippage. The work in [6] proposed a fuzzy cluster means (FCM) technique to fuse multiple IMUs to produce a robust measurements that is utilized in INS mechanization integrated with GPS. The results in this work show significant improvement when using FCM with multi-IMU structure over using only one. Furthermore, the work in [23] utilized the ANFIS model to predict the dual-mass MEMS gyroscope's output drift caused by the temperature. While the work in [24] utilized the ANFIS model to enhance the navigation solution of the INS by training the ANFIS model by a differential GPS data set as a reference position and evaluating the model on a public raw data set (KITTI) with a trajectory that lasts between (140-300)s. Furthermore, the work in [25] utilized the ANFIS model as a solution for the navigation problem of a mobile robot.

The work in [26] utilizes empirical mode decomposition threshold filtering (EMDTF) and a long-short-term memory (LSTM) neural network. The EMDTF disposes the noise generated in the INS's sensors while the LSTM uses to predict the pseudo-GPS position during GPS outages. The presented EMDTF scheme improves the accuracy of east velocity, north velocity, longitude, and latitude by 9.12%, 15.14%, 13.78%, and 10.72% respectively. Whilst, the LSTM scheme reduces the RMSE by 21.79%, 14.85%, 55.03%, and 19.66% over the traditional artificial neural networks. Moreover, The work in [27] overcome the dilemma of poor navigation accuracy in challenging environments by proposing a fusion scheme utilizing machine learning techniques. The proposed scheme utilizes the support vector regression-based adapted Kalman filter (SVR-AKF) to regulate the covariance parameters

Preprints (www.preprints.org) | NOT PEER-REVIEWED | Posted: 16 February 2022 doi:10.20944/preprints202202.0193.v1

of the KF. In addition, the adaptive neuro-fuzzy inference system (ANFIS) is used to predict the navigation solution errors of the INS during the GNSS outages. The proposed scheme is compared with the traditional schemes using the KF and EKF over two real trajectories. The results show that an improvement in the over position error about 58.8% against the KF over trajectory one and 48% to 67.5% against the KF and 34.2% to 57.6% against the EKF over trajectory two.

A recent survey about the ML techniques and how they can be involved in all fundamental steps in the inertial-sensing applications to improve the navigation solution obtained from the INS was introduced in [28], stating the advantages and the challenges of utilizing them. The authors mentioned several challenges facing the use of ML with the inertial sensors such as the nonexistence of hardware combination between the inertial sensors and ML and the shortage of work on the sensors measurements improving using ML. In addition, the authors mentioned that the use of ML over the sensors measurements is a promising field of research and most of the work conducted ML is applied only to the INS navigation solution.

From the previous related work discussion, it's been noticed that most of the presented research utilized the ML techniques over the INS solution, not the inertial sensors measurements. Therefore, in this paper, we propose an ANFIS algorithm to be applied to the raw measurements of a commercial IMU to leverage its performance. This process is carried out using a high-end IMU as a reference to provide a suitable model for the low-end one in ML structure. The model is generated in the training phase using both IMUs then applied to the low-end IMU in the testing phase. The proposed ML algorithm has been evaluated on a real road trajectory. The results show a significant improvement of the commercial IMU measurements as well as the INS navigation solution compared to the traditional INS solution. The contributions of this research paper are summarized as follows:

1. Development of an ML-based-ANFIS algorithm as a ML technique to leverage the grade of a low-grade IMU.
2. Comparing the low-grade IMU measurements before and after applying the proposed algorithm to the reference IMU.
3. Validation of the proposed algorithm by applying the tested IMU data to INS mechanization.

The paper is organized into six sections. In Section I, the introduction, related work, and paper contributions are discussed. Section II concludes a background about the INS and the ANFIS algorithm. The methodology is explained in Section III. The experimental setup and the utilized units are detailed in Section IV. The results are discussed in Section V. Finally, the paper is concluded in Section VI.

2. Background

2.1. Inertial Navigation Systems

The traditional inertial navigation system is composed of IMU and a navigation processor. The IMU composed of 3 accelerometers provides the specific forces, and 3 gyroscopes provide the angular rates [1,29–31] as shown in Fig. 1. The INS depends on the knowledge of the target's initial states (position, velocity, and attitude (PVA)) and updates its current states accordingly, as shown in Eq. (1), (2), and (3).

The mechanization process of the INS can be summarized in three main steps. First, we obtain the angular rates $(\omega_x, \omega_y, \omega_z)$ from the gyroscopes and the accelerations(f_x, f_y, f_z) from the accelerometers, and obtaining the attitude angles of pitch, roll, and yaw (p, r, y) from the angular rates after calculating the transformation matrix. Second, with the assistance of the rotation matrix, the forces in the navigation frame from the body frame can be obtained and then transformed to the local-level frame (LLF). Finally, the velocity is obtained by integrating the transformed forces, and the position is obtained by integrating the calculated velocity [1,32].

Preprints (www.preprints.org) | NOT PEER-REVIEWED | Posted: 16 February 2022 doi:10.20944/preprints202202.0193.v1

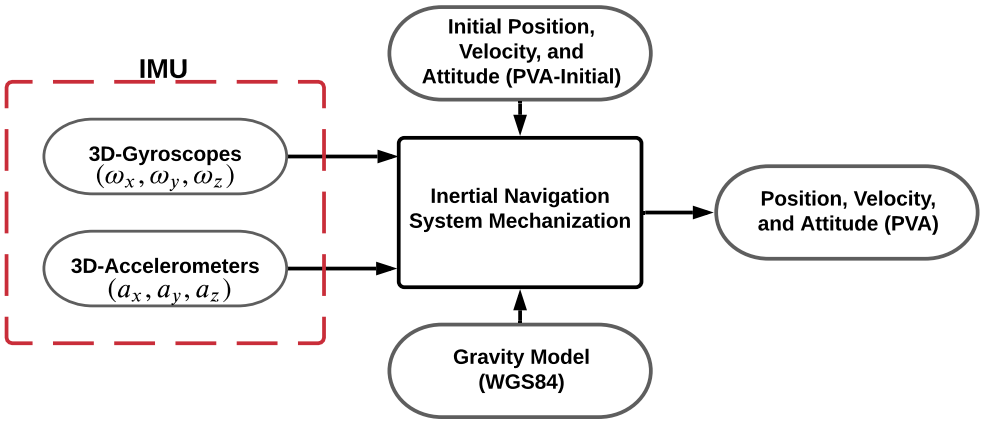

Figure 1. Strap down INS block diagram

$$Position = [\varphi \ \ \lambda \ \ h]^T \tag{1}$$

Where; φ is the latitude, λ is the longitude and h is the altitude.

$$Velocity = [V_N \ V_E \ V_D]^T \tag{2}$$

Where; $V_N$is the north velocity, V_E is the east velocity, and V_D is the down velocity.

The attitude provided is as shown in Eq.(3).

$$Attitude = [q_o \ q_1 \ \ q_2 \ \ q_3]^T \tag{3}$$

Where; the quaternions are the parameterization of the rotation matrix.
The attitude rates are calculated as Eq.(4).

$$\begin{bmatrix} \dot{q_0} \\ \dot{q_1} \\ \dot{q_2} \\ \dot{q_3} \end{bmatrix} = 0.5 \begin{bmatrix} 0 & \omega_x & -\omega_y & -\omega_z \\ \omega_x & 0 & \omega_z & -\omega_y \\ \omega_y & -\omega_z & 0 & \omega_x \\ \omega_z & \omega_y & -\omega_x & 0 \end{bmatrix} \begin{bmatrix} q_0 \\ q_1 \\ q_2 \\ q_3 \end{bmatrix} \tag{4}$$

Also, the quaternion attitude can be transferred to Euler's angles roll, pitch, and yaw respectively as in Eq.(5).

$$\begin{bmatrix} \phi \\ \theta \\ \psi \end{bmatrix} = \begin{bmatrix} atan2(2\, q_2 q_3 + 2 q_1 q_0 \,), (q_3^2 + q_0^2 - q_1^2 - q_2^2)) \\ -asin(2\, q_1 q_3 - 2 q_2 q_0 \,) \\ atan2((2\, q_1 q_2 + 2 q_0 q_3 \,), (q_0^2 + q_1^2 - q_2^2 - q_3^2)) \end{bmatrix} \tag{5}$$

Where; ϕ is the Roll angle in radian, θ is the Pitch angle in radian, ψ is the Yaw angle in radian.

Eq.(6) shows the transformation matrix from the body frame to LLF using quaternion states [33].

$$C_b^n = \begin{bmatrix} q_1^2 + q_o^2 - q_2^2 - q_3^2 & 2(q_1 q_2 - q_3 q_o) & 2(q_2 q_3 + q_2 q_o) \\ 2(q_1 q_2 + q_3 q_o) & q_2^2 + q_o^2 - q_1^2 - q_3^2 & 2(q_2 q_3 - q_1 q_o) \\ 2(q_1 q_3 - q_2 q_o) & 2(q_2 q_3 + q_1 q_o) & q_3^2 + q_o^2 - q_1^2 - q_2^2 \end{bmatrix} \tag{6}$$

The specific forces can be transformed into LLF using the transformation matrix C_b^n, and are obtained as in Eq.(7).

Preprints (www.preprints.org) | NOT PEER-REVIEWED | Posted: 16 February 2022 doi:10.20944/preprints202202.0193.v1

$$\begin{bmatrix} F_N \\ F_E \\ F_D \end{bmatrix} = C_b^n \begin{bmatrix} f_x \\ f_y \\ f_z \end{bmatrix} \tag{7}$$

The velocity rates can be obtained as in Eq.(8).

$$\begin{bmatrix} \dot{V}_N \\ \dot{V}_E \\ \dot{V}_D \end{bmatrix} = \begin{bmatrix} 1 & 0 & 0 & 0 & -(\dot{\lambda} + 2w_e sin(\varphi)) & \dot{\varphi} & 0 \\ 0 & 1 & 0 & (\dot{\lambda} + 2w_e sin(\varphi)) & 0 & (\dot{\lambda} + 2w_e cos(\varphi)) & 0 \\ 0 & 0 & 1 & -\dot{\varphi} & -(\dot{\lambda} + 2w_e cos(\varphi)) & 0 & 1 \end{bmatrix} \begin{bmatrix} F_N \\ F_E \\ F_D \\ V_N \\ V_E \\ V_D \\ g \end{bmatrix} \tag{8}$$

Where; $\dot{\lambda}$ and $\dot{\varphi}$ are the longitude and latitude rates, respectively, $w_e = 7.2921158 \times 10^{-5}$rad/s is the magnitude of the rotating rate of the Earth and g is the gravity which can be obtained as shown in Eq.(9).

$$g = g_{WGS0)} \frac{1 + g_{WGS1} sin(\varphi)}{[1 - E^2 sin^2(\varphi)]^{\frac{1}{2}}} - \left[3.0877 \times 10^{-6} - 0.0044 \times 10^{-6} sin^2(\varphi)\right] h + 0.072 \times 10^{-12} \tag{9}$$

Where; $g_{WGS0} = 9.78032677\ m/s^2$ is the gravity at the equator, $g_{WGS1} = 0.00193185138639\ m/s^2$ is the gravity formula constant, and $E^2 = 0.0818191908426$ is the first eccentricity. The position rates are obtained as in Eq.(10).

$$\begin{bmatrix} \dot{\varphi} \\ \dot{\lambda} \\ \dot{h} \end{bmatrix} = \begin{bmatrix} \frac{V_N}{R_M + h} \\ \frac{V_E}{(R_N + h) cos(\varphi)} \\ -V_D \end{bmatrix} \tag{10}$$

Where; R_M and R_N are the meridian radius and normal radius of the Earth's ellipsoid model, respectively.

Unfortunately, the INS suffers from error growth over time because of the two times integration process of the target's acceleration. The errors in the INS can be categorized and divided into deterministic and stochastic errors. The deterministic errors include bias offset, scale factor, and axis misalignment errors. In contrast, the stochastic errors include bias drift, bias stability, scale factor stability, noise, and axes misalignment errors. The deterministic errors can be reduced or compensated if the sensors are properly calibrated, especially high-end sensors, while the stochastic errors are modeled randomly to reduce their effect. So, the gyroscope measurement model is represented in Eq.(11).

$$\widetilde{\omega}_{ib}^b = \omega_{ib}^b + b_g + S\omega_{ib}^b + N\omega_{ib}^b + \varepsilon_g \tag{11}$$

Where; $\widetilde{\omega}_{ib}^b$ is the gyroscope measurement vector, ω_{ib}^b is the true angular rate velocity vector, b_g is the gyroscope instrument bias vector, S_g is a matrix representing the gyro scale factor, N_g is a matrix representing non-orthogonality of the gyro triad, ε_g is the vector representing the gyro sensor noise.

Furthermore, the accelerometers measurement model is represented in Eq.(12).

$$\widetilde{f}^b = f^b + b_a + S_1 f + S_2 f^2 + N_a f + \delta_g + \eta_g \tag{12}$$

Where; $\widetilde{f}^b$ is the accelerometer measurement vector, f^b is the true specific force vector, b_a is the accelerometer instrument bias vector, S_1 is a matrix of the linear scale factor error, S_2 is a matrix of the non-linear scale factor error, N_a is a matrix representing non-orthogonality of the accelerometer's triad, δ_g is the anomalous gravity vector, η_g is a vector representing the accelerometer sensor noise.

The classification of the INS systems depends on the IMU accuracy and its ability to reduce the error growth over time. Therefore, the need to compensate for the low-cost

Preprints (www.preprints.org) | NOT PEER-REVIEWED | Posted: 16 February 2022 doi:10.20944/preprints202202.0193.v1

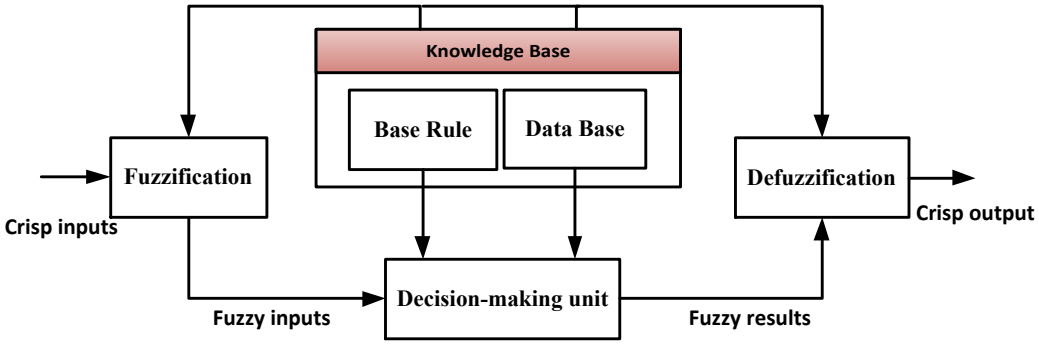

Figure 2. The structure of the Fuzzy inference system

commercial IMUs' errors has been elevated by applying either traditional techniques or ML techniques to enhance the INS's navigation solution.

2.2. *Adaptive Neuro-Fuzzy Inference System (ANFIS)*

The adaptive neuro-fuzzy inference system (ANFIS) is a fusion technique between the artificial neural network (ANN) and the fuzzy inference system (FIS). Subsequently, it provides the advantages of both techniques and overrides their disadvantages. It obliges the system towards adaptation through the self-organizing and self-learning process [34].

The main structure of the FIS is shown in Fig.2. The FIS is based on the fuzzy conditional statements (if-then rule) in which is responsible for making the decisions in an environment of impressions and uncertainty [35]. The structure of the FIS is composed of five main blocks. The fuzzification process switches the crisp inputs into data sets by applying the membership function (MF). The base rule contains the fuzzy if-then rules and the database comprises the MF utilized in the fuzzy rules. The decision-making unit executes the inference operation on the fuzzy rules. The defuzzification process turns the fuzzy results into a crisp output [36–38].

Similarly, the ANFIS's functionality is equivalent to the FIS, as shown in Fig.3[39]. The ANFIS structure is composed of five layers. At the first layer, each node assigns the crisp inputs after applying the MF. The output of this layer clarifies how much the input fulfills the linguistic label as in Eq.(13) [35,37].

$$O_i^1 = \mu_{A_i}(x) \tag{13}$$

Where; X is the input to node i, A_i is the linguistic label for input X.

The second layer multiplies the input signals at each node to obtain the rules' weights (firing strength) as in Eq.(14).

$$W_i = \mu_{A_i}(x) \times \mu_{B_i}(y) \tag{14}$$

Where; x, y are the two inputs, A_i is the linguistic label for input X, and B_i is the linguistic label for input y. The third layer normalizes the weights of each rule by computing the ratio of the weight of each rule to the sum of all the rules' weights as in Eq.(15).

$$\widetilde{W} = \frac{W_i}{\sum W} \tag{15}$$

At the fourth layer, the normalized weights of each rule are multiplied by the output of the second layer as in Eq.(16).

$$O_i^4 = \widetilde{W_i} f_i = \widetilde{W_i}(p_i x + q_i y + r_i) \tag{16}$$

Preprints (www.preprints.org) | NOT PEER-REVIEWED | Posted: 16 February 2022 doi:10.20944/preprints202202.0193.v1

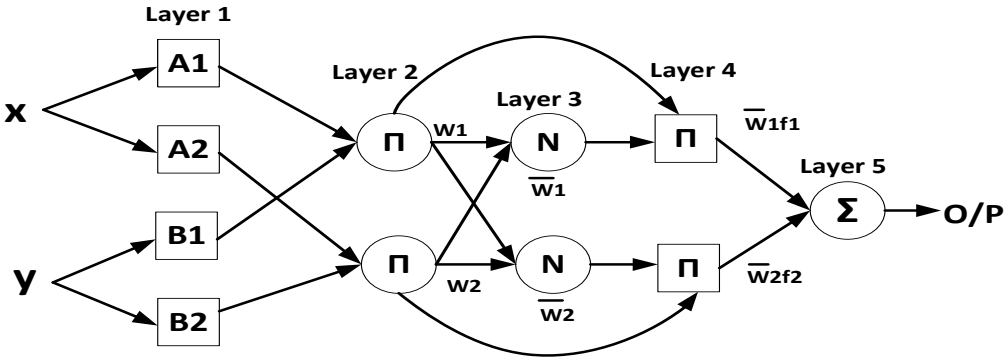

Figure 3. The ANFIS system structure [39]

Where; $\widetilde{W_i}$ is the normalized weight obtained from the third layer, p_i, q_i, and r_i are called consequent parameters.

Finally, the fifth layer sums all the incoming signals to compute the overall output as in Eq.(17).

$$Overall = \sum_i \widetilde{W} f_i = \frac{\sum_i W_i f_i}{\sum_i W_i} \tag{17}$$

3. Methodology

As mentioned in the previous section, the accuracy of the INS's navigation solution depends upon the quality/grade of the IMU sensors and the ability to compensate for its sensors' errors. In this paper, we exploit the capability of the ML-ANFIS technique to estimate the inertial sensors' errors by training a low-grade IMU with a high-end one. This work aims to boost low-grade IMU performance.

The proposed ML technique is composed of two phases, the training phase, and the testing phase. The training phase block diagram is shown in Fig.4. In this phase, the training data set consists of the low-grade IMU's sensors measurement as an input and the high-grade IMU as output. This phase is carried out using half of the trajectory data. At the most, the Gaussian and the Triangular MFs. The Triangular membership function is chosen to be the input and output membership function. Vastly, the Triangular MF is utilized for its naivety and is faster than the Gaussian MF for the computation. The clustering method utilized is the 'Grid-partition' in which every input variable equally distributed input MF and generates a single-output Sugeno-fuzzy system. The number of MFs is six, each for the six IMU sensor measurements. Subsequently, the rule base contains one rule for every input MF combination. The output MF is linear which the output of every rule is a linear function of the input variables, scaled by the previous result value. The testing phase is shown in Fig.5. The ML-model generates its predicted IMU measurements (Six sensors' measurements) to obtain the position, velocity, and attitude (PVA). Then, the navigation solution of the ML-model is compared to the navigation solution of the reference to obtain ΔPVA of the ML-model. Similarly, the navigation solution of the low-grade IMU is compared to the navigation solution of the reference to obtain ΔPVA of the low-grade IMU. The differences in errors in the navigation solution between the ML-model and low-grade IMU are calculated to compute the influence of the ML-model in enhancing the navigation solution of a low-grade IMU's sensors measurement, which will be shown in the upcoming sections. The overall algorithm is explained in Table 1 in a pseudo-code form.

Preprints (www.preprints.org) | NOT PEER-REVIEWED | Posted: 16 February 2022 doi:10.20944/preprints202202.0193.v1

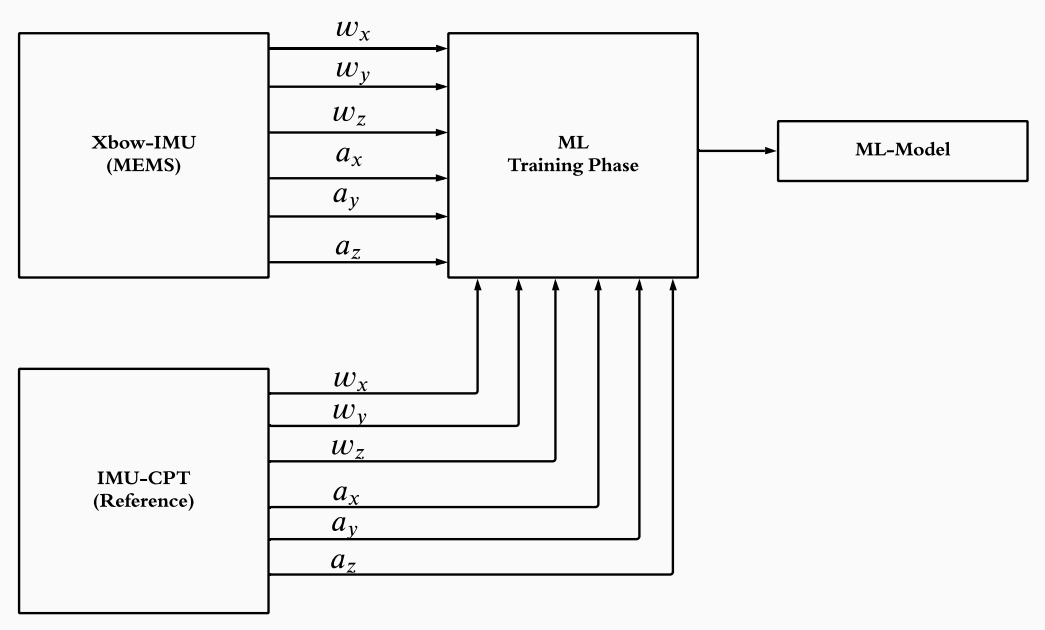

Figure 4. The training phase of the ML-based-ANFIS

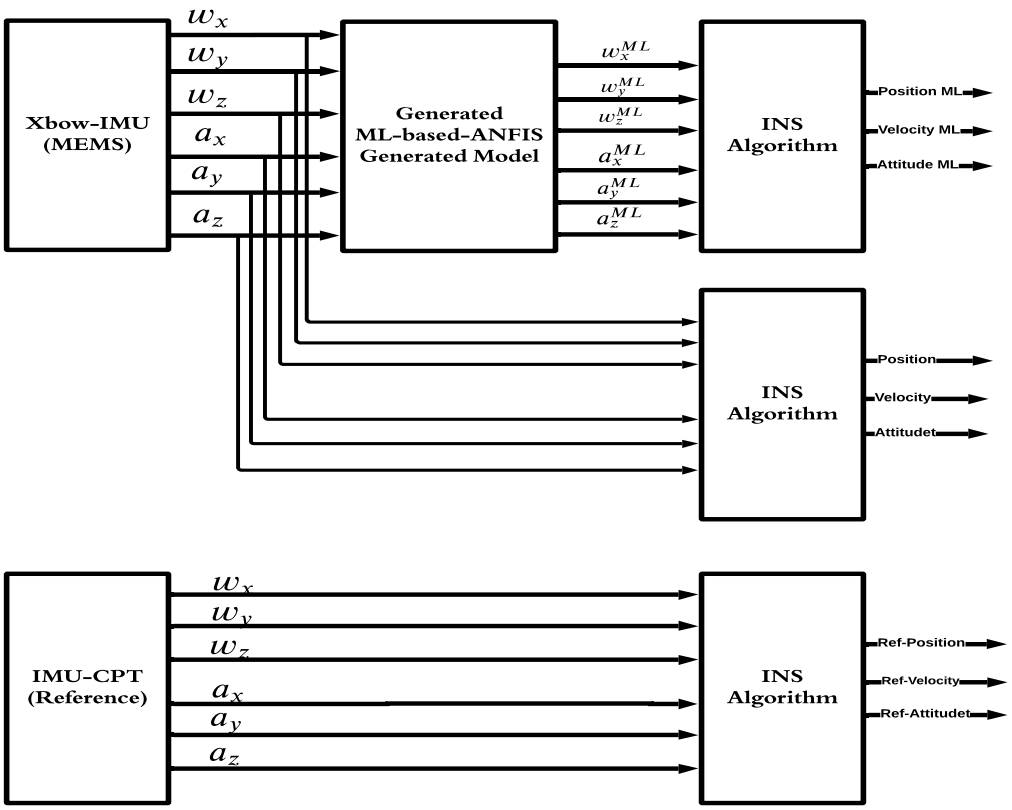

Figure 5. The testing phase of the ML-based-ANFIS

Preprints (www.preprints.org) | NOT PEER-REVIEWED | Posted: 16 February 2022 doi:10.20944/preprints202202.0193.v1

Table 1: ML-ANFIS Algorithm for INS Improvement

Algorithm INS solution improvement using ML	
Input	IMU's sensors measurements 3 gyroscopes and 3 accelerometers $(\omega_x,\ \omega_y,\ \omega_z,\ a_x,\ a_x,\ a_x)$ for the MEMS-IMUand the reference IMU, Initial PVA states $(Lat_0,\ Long_0, Att_0, V_0^N, V_0^E, V_0^D,\ p_0, r_0, y_0)$ and the navigation solution of the reference IMU $(pos\_ref, vel\_ref, att\_ref)$.
Step 1	Prepare and tune the ML-ANFIS options (input data, output data, type of clustering, MF's type, number of MF and epochs/iterations).
Step 2	Apply the ML-ANFIS (**The training phase**) on half of the input data (50%).
Step 3	Generate the ML-ANFIS.
Step 4	Evaluate and apply the ML-ANFIS on the remaining data (**the testing phase**).
Step 5	Evaluate the ML-ANFIS's output (improved IMU's sensors measurements $(\omega_x, \omega_y, \omega_z, a_x, a_y, a_z)$.
Step 6	Compare the MEMS IMU's sensors measurements and the ML-ANFIS IMU's sensors measurements to the reference IMU's sensors measurements to compute the percentage of improvement caused by ML-ANFIS (RMSE). $RMSE = \sqrt{\frac{1}{n}\sum_n \left(X_{n,Ref} - X_{n,ML}\right)^2}$ Where; $X_{n,Ref}$ and $X_{n,ML}$ are the reference IMU and trained IMU measurements respectively.
Step 7	Compute the ML-ANFIS's navigation solution (PVA) by using the output of ML-ANFIS as an input to the INS.
Step 8	Compare MEMS IMU (PVA) and the ML-ANFIS (PVA) to the reference IMU (PVA) to compute the percentage of improvement of the ML-ANFIS (PVA) using the RMSE metric.
Output	The INS solution (PVA) of the MEMS-IMU and the ML-model compared to the output using the reference IMU.

4. EXPERIMENTAL SETUP

The experimental work was carried out to verify the effectiveness of the ML model through a real road test trajectory. The IMUs utilized in the experimental work were set up inside the test van are shown in Fig.6. The testbed was installed inside the van, coinciding with its axes. Furthermore, utilizing a standard seat chassis, the testbed was rigidly and firmly settled in the rear seat location. The low-grade IMU sensor utilized in this research was the Crossbow MEMS grade XBOW IMU300CC and the high-grade IMU utilized as a reference was the IMU-CPT which includes three MEMS accelerometers and three fiber-optic gyroscopes (FOG). The specifications of the two IMU units can be found in Table 2.

5. RESULTS AND DISCUSSION

A real road trajectory was conducted to test the proposed ML-technique performance in the downtown area of Kingston, ON, Canada. The reference trajectory is the INS solution that utilized the IMU-CPT sensors' measurements as a control input to the IMS mechanization. Moreover, the trajectory lasted for 2300 seconds (almost 44 minutes) and contained various maneuvers at different speeds.

The application of the ML-based-ANFIS over the XBOW IMU measurements is carried out in two stages. The first stage is the training stage, in which the IMU-CPT is utilized as a learning source. This stage is applied over 50% of the data to generate the ML-based-ANFIS model. Three gyroscopes and three accelerometers were trained in this stage to produce a suitable model. The ML-based-ANFIS utilized six-membership functions with adaptive step size. In the results shown in figures 7 to 15, the reference is designated by red color, the XBOW-IMU in blue, and the proposed ML-based-ANFIS in green for both row measurements and INS solution comparisons.

The 3D-Gyroscopes and accelerometers measurements in the training stage are shown in Fig.7 and Fig.8 respectively.

Preprints (www.preprints.org) | NOT PEER-REVIEWED | Posted: 16 February 2022 doi:10.20944/preprints202202.0193.v1

Table 2: Utilized IMUs PERFORMANCE CHARACTERISTICS

IMUs	IMU300CC(XBOW) (100HZ)	IMU-CPT (100HZ)
Size (cm^3)	7.62×9.53×3.2	15.2×16.8×8.9
Weight	0.59 Kg	2.28 Kg
Max data rate	200 Hz	100Hz
Start-up time	<1 sec	<5 sec
Accelerometer		
Range	±2 g	±10 g
Bias instability	±30 mg	±0.75 mg
Scale factor	<1%, 1σ	300ppm, 1σ
Gyroscope		
Range	±100 °/s	±375 °/s
Bias instability	<±2.0 °/s	±1.0 °/h
Scale factor	<1 %, 1σ	1500ppm,1σ

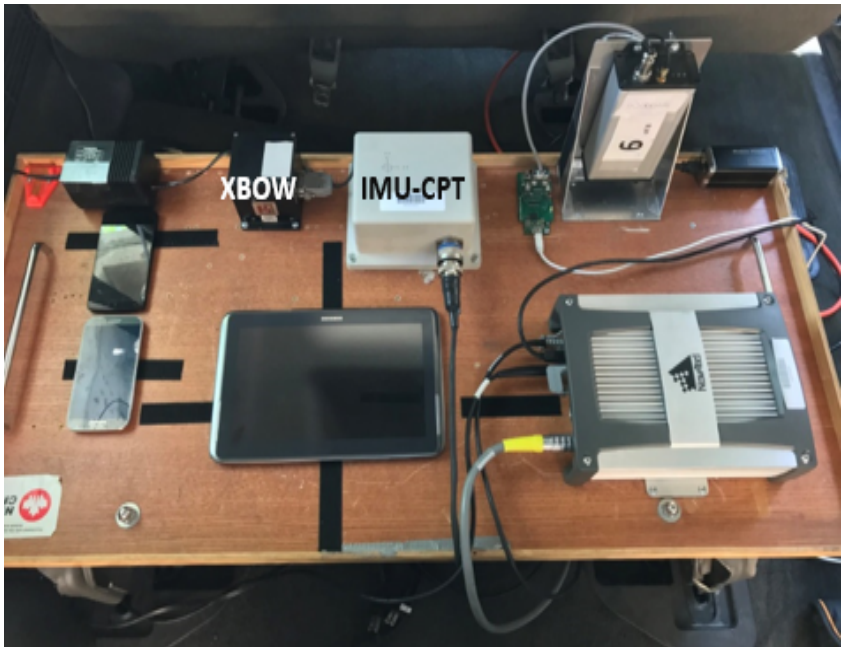

Figure 6. The Utilized IMUs mounted on the testbed

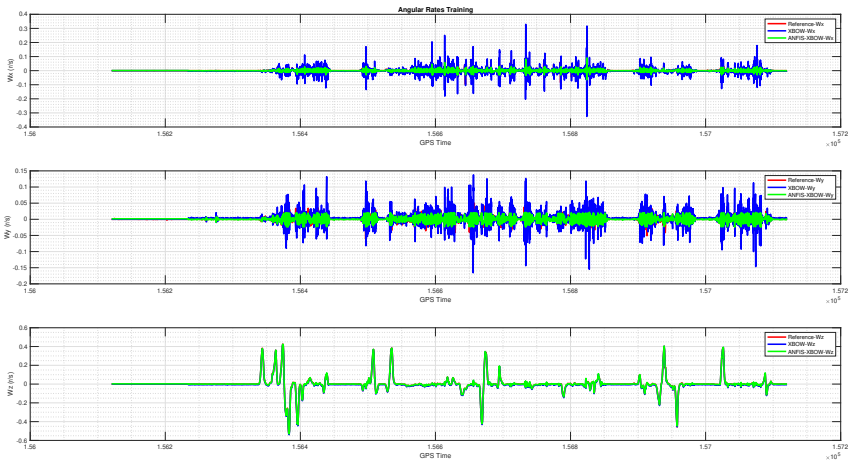

Figure 7. 3D-Gyroscopes angular rates with ML-based-ANFIS (Training Stage)

Preprints (www.preprints.org) | NOT PEER-REVIEWED | Posted: 16 February 2022 doi:10.20944/preprints202202.0193.v1

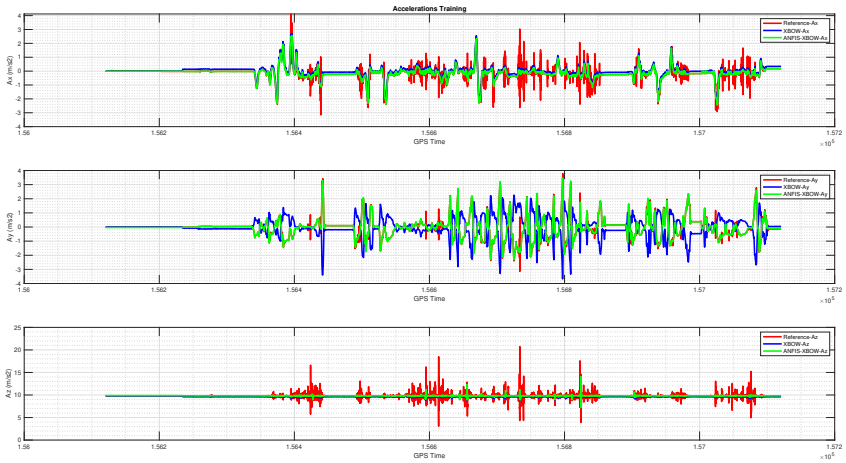

Figure 8. 3D-Accelerometers with ML-ANFIS (Training Stage)

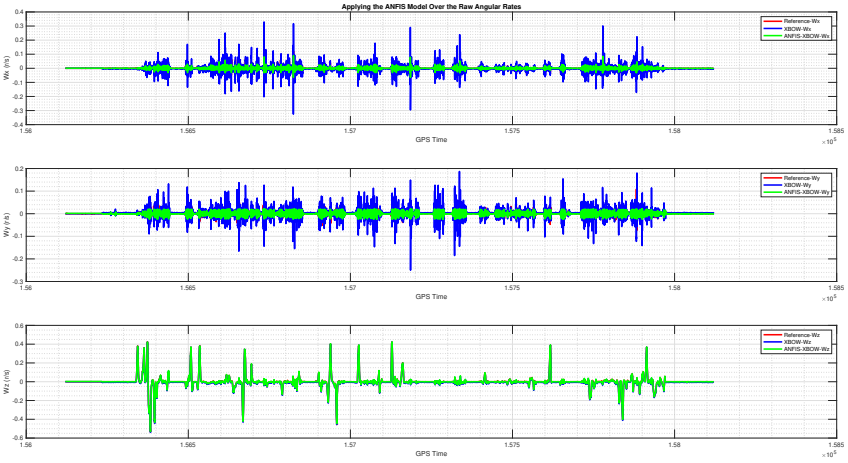

Figure 9. 3D-Gyroscopes angular rates after applying the ML-based-ANFIS (Testing Stage)

The generated ML-based-ANFIS model is then applied to the remaining XBOW-IMU measurements. This step is the testing stage where the generated model is applied and its performance is measured.

Fig.9 shows a comparison between the row XBOW-IMU gyroscopes measurements in 3 directions (x, y, and z) and those with the applied ML model compared to the reference angular rates from the IMU-CPT. A zoomed-in view for a portion of the testing data is shown in fig.10. The results in fig.10 show that the biases and scale factor and a significant part of the associated noise have been removed when applying the proposed ML technique over the low-grade IMU gyros measurements. The accelerations' comparison for the testing part is shown in fig.11. Additionally, a zoomed-in view for the accelerations in this stage is shown in fig.12. The results show the proposed ML technique's ability to estimate and remove the errors associated with the low-grade IMU measurements. Also, it's noticed that not only the noise is mainly removed, but both bias and scale factor errors were also reduced significantly.

Therefore, the produced IMU measurements from the proposed ML technique application provide a more robust input to the INS mechanization, which leads to a more accurate navigation solution.

To validate the resulted measurements, a comparison of the XBOW-IMU raw measurements before and after applying the proposed ML technique is shown in Table 3 using

Preprints (www.preprints.org) | NOT PEER-REVIEWED | Posted: 16 February 2022 doi:10.20944/preprints202202.0193.v1

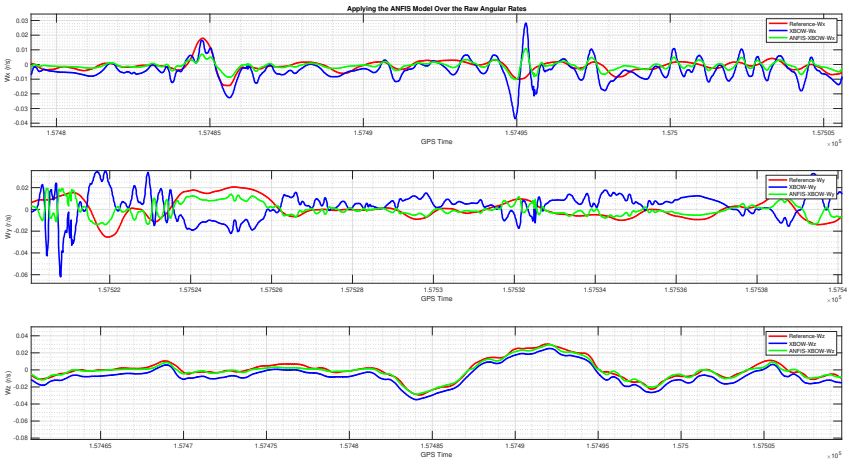

Figure 10. A zoomed-in part of the IMU Gyro measurements

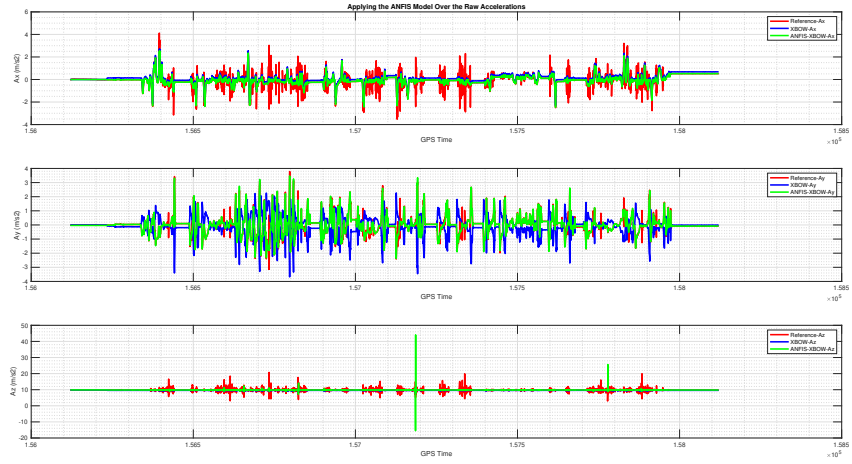

Figure 11. 3D-Accelerometers with ML-based-ANFIS (Testing Stage)

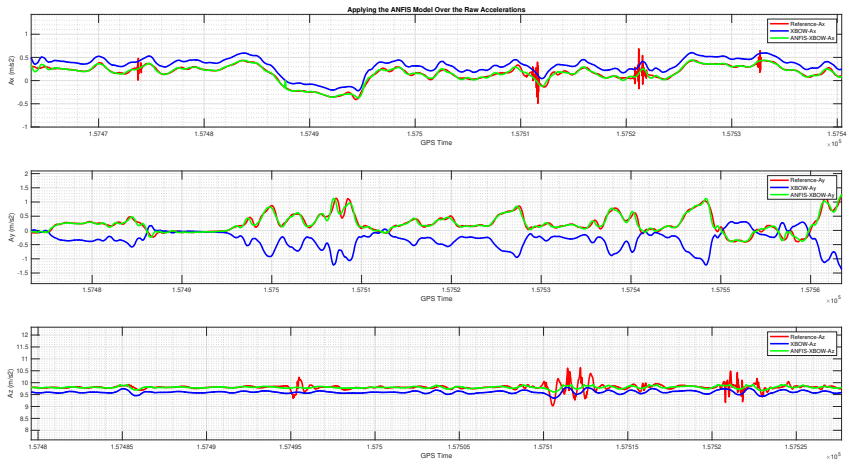

Figure 12. A zoomed-in part of the IMU accelerometers

Preprints (www.preprints.org) | NOT PEER-REVIEWED | Posted: 16 February 2022 doi:10.20944/preprints202202.0193.v1

Table 3: IMU Raw Measurements RMSE Comparison

RMSE	ω_x	ω_y	ω_z	a_x	a_y	a_z
XBOW	0.0158	0.0213	0.0064	0.1902	1.2629	0.3542
ML-XBOW	0.0084	0.0069	0.0026	0.1084	0.0757	0.2873

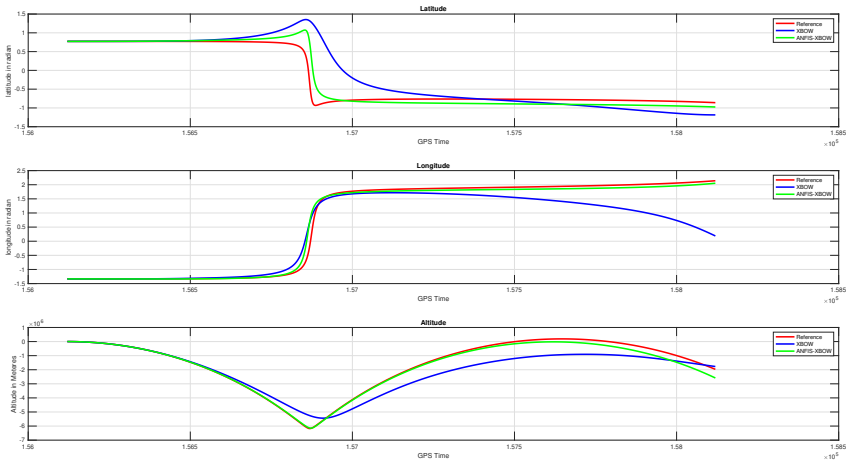

Figure 13. Position (Lat, Long, and Alt) components comparison

the RMSE for each measurement. The results show significant improvement of the IMU measurements when using the ML-based-ANFIS.

The output of this process is new IMU measurements that are ready to be applied to the INS algorithm. Consequently, to verify the performance of the proposed ML-based-ANFIS, the modified and unmodified measurements are applied to the INS algorithm to produce the navigation information PVA. The output PVA is then compared to the reference PVA to check the improvement and the worthiness of using ML in training the raw MEMS-IMU measurements by a high-end IMU.

The results show the produced INS solution from the XBOW IMU (low-grade) and the corresponding modified measurements (ML-based-ANFIS) when using the proposed ML technique compared to the reference solution from the IMU-CPT.
The position components (Latitude in radians, Longitude in radians, and Altitude in meters) comparison is shown in Fig.13. The results show that the position components when using the proposed ML technique are closer to the reference position components compared to the ones when using the XBOW IMU raw measurements. Therefore, the utilization of ML in improving the IMU measurements leverages the position solution of the unit. The velocity components in the navigation frame (V_N, V_E, and V_D) comparison are shown in Fig.14. It's noticeable that there is a significant improvement in all the velocity components when using the proposed ML technique. A comparison of the attitude components (Roll, Pitch, and Yaw) angle is shown in Fig.15 illustrating significant improvement of the attitude components solution. A statistical analysis of the INS solution position and velocity components from the testing part of the trajectory (24 minutes) is shown in Table 4. A 70% overall improvement of the 2D-position and 92% improvement of the 2D-velocity have been achieved when using the proposed ML-based-ANFIS technique. Also, the attitude components had a great improvement. The roll angles RMSE have been reduced from 55.6 degrees to 6 degrees with an improvement of 89.2%, the pitch angles RMSE reduced from 42.6 degrees to 6.5 degrees with an improvement of 84.7%, and the yaw angles reduced from 86.3 degrees to 79.3 degrees with an improvement of 8%. The yaw angles improvement percentage is less than other attitude components due to the proximity of the row w_z to the reference w_z as shown in fig.9 and fig.10. The results show the superiority

Preprints (www.preprints.org) | NOT PEER-REVIEWED | Posted: 16 February 2022 doi:10.20944/preprints202202.0193.v1

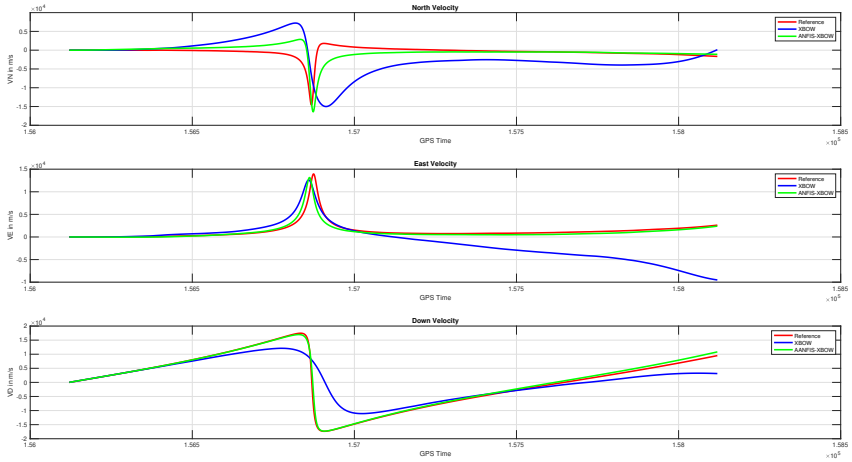

Figure 14. Velocity (V_N, V_E, and V_D) components comparison

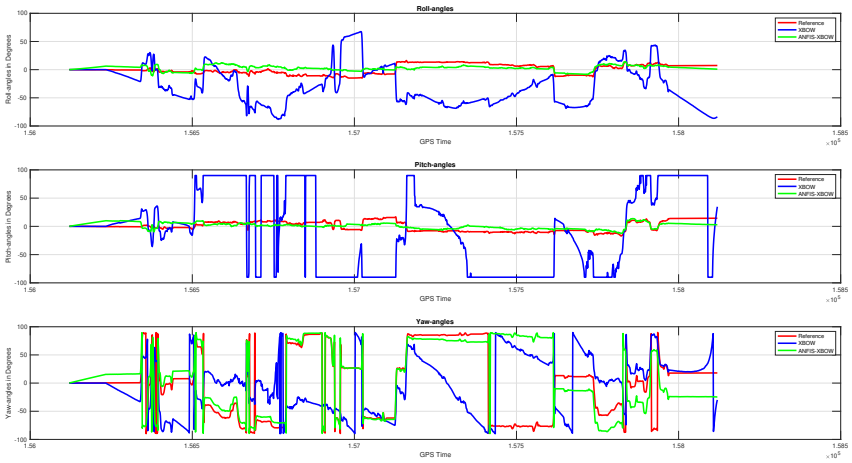

Figure 15. Attitude (Roll, Pitch, and Yaw) angles comparison

Table 4: Results Analysis Over the Testing Part of the Trajectory (24 minutes)

Units		XBOW	ML-XBOW
Position RMSE (m)	North	311,899.4	222,857.2
	East	732,549.2	83,613.3
	Down	967,706.2	291,313.6
	2D-Pos	796,184.3	238,026.2
	3D-Pos	1,253,141.9	376,191.6
Velocity RMSE (m/s)	VN	2,730.5	360.5
	VE	5,879.4	338.9
	VD	2,242.8	655.2
	2D-Vel	6,482.5	494.8
	3D-Vel	6,859.5	821
Attitude RMSE (Deg)	Roll	55.6	6.09
	Pitch	42.6	6.5
	Yaw	86.3	79.3

 doi:10.20944/preprints202202.0193.v1

of applying the ML to leverage the low-grade IMU, which significantly enhances the INS navigation solution compared to the traditional solution using the row measurements of the low-grade IMU.

6. CONCLUSIONS AND FUTURE WORK

This paper has discussed the utilization of ML-based-ANFIS in improving MEMS-grade IMU raw measurements. The proposed ML algorithm is applied to real data collected with a low-cost IMU. The proposed ML technique is applied to 50% of the collected data and tested on the remaining data. The output of this process is then applied to a strap-down INS to produce a navigation solution PVA. The produced navigation solution achieved a 2D-position improvement of 70% and 2D- velocity improvement of 92%. Also, an improvement of 89.2%, 84.7%, and 8% of the attitude components roll, pitch, and yaw, respectively, have been achieved. The work in this paper shows that using ML in boosting a low-grade IMU has a significant impact on the inertial sensors' performance. Moreover, it has a great impact on producing a more accurate and robust INS navigation solution. As a future step, this work can be combined with either another ML technique or EKF for bridging the GNSS outages in GNSS challenging environments.

Author Contributions: A.A. (Ahmed Mahdi) proposed the algorithm, performed the experiments, and wrote the manuscript; A.A.(Ahmed Azouz) reviewed the manuscript and provided important suggestions to improve the algorithm; A. A. (Ahmed Abdalla) revised the manuscript; A.A. (Ashraf Abosekeen) participated in preparing the algorithm, the experimental work, results analysis, and wrote and revised the manuscript.

Funding: This research received no external funding.

Institutional Review Board Statement:

Informed Consent Statement:

Data Availability Statement:

Acknowledgments:

Conflicts of Interest: The authors declare no conflict of interest.

References

1. Noureldin, A.; Karamat, T.B.; Georgy, J. *Fundamentals of Inertial Navigation, Satellite-based Positioning and their Integration*; Vol. 1, Springer Berlin Heidelberg: Berlin, Heidelberg, 2013; p. 313. doi:10.1007/978-3-642-30466-8.
2. Abosekeen, A.; Iqbal, U.; Noureldin, A.; Korenberg, M.J. A Novel Multi-Level Integrated Navigation System for Challenging GNSS Environments. *IEEE Transactions on Intelligent Transportation Systems* **2021**, *22*, 4838–4852. doi:10.1109/TITS.2020.2980307.
3. Li, Y.; Chen, R.; Niu, X.; Zhuang, Y.; Gao, Z.; Hu, X.; El-Sheimy, N. Inertial Sensing Meets Artificial Intelligence: Opportunity or Challenge? *arXiv* **2020**, [2007.06727].
4. Abosekeen, A.; Noureldin, A.; Karamat, T.; Korenberg, M.J. Comparative Analysis of Magnetic-Based RISS using Different MEMS-Based Sensors. the 30th International Technical Meeting of the Satellite Division of the Institute of Navigation (ION GNSS+ 2017); Raquet, J.; Kassas, Z., Eds.; Inistitute of Navigation: Portland, Oregon, 2017; pp. 2944 – 2959. doi:10.33012/2017.15120.
5. Abosekeen, A.; Iqbal, U.; Noureldin, A. Improved Navigation Through GNSS Outages: Fusing Automotive Radar and OBD-II Speed Measurements with Fuzzy Logic. *GPS World* **2021**, *32*, 36–41.
6. Abosekeen, A.; Abdalla, A. Improving the Navigation System of a UAV Using Multi-Sensor Data Fusion Based on Fuzzy C-Means Clustering. *International Conference on Aerospace Sciences and Aviation Technology* **2011**, *14*, 1–12. doi:10.21608/asat.2011.23432.
7. Abosekeen, A.; Iqbal, U.; Noureldin, A. Enhanced Land Vehicles Navigation by Fusing Automotive Radar and Speedometer Data. 33rd International Technical Meeting of the Satellite Division of the Institute of Navigation (ION GNSS+ 2020); , 2020; pp. 2206–2219. doi:10.33012/2020.17527.
8. Abosekeen, A.; Abdalla, A. Fusion of Low-Cost MEMS IMU/GPS Integrated Navigation System. The 8th International Conference on Electrical Engineering; M.T.C., Ed.; M.T.C: Cairo, 2012; Vol. 8, pp. 1–23. doi:10.21608/iceeng.2012.30810.
9. Rashed, M.A.; Abosekeen, A.; Ragab, H.; Noureldin, A.; Korenberg, M.J. Leveraging FMCW-radar for autonomous positioning systems: Methodology and application in downtown Toronto. Proceedings of the 32nd International Technical Meeting of the Satellite Division of the Institute of Navigation, ION GNSS+ 2019; , 2019; pp. 2659–2669. doi:10.33012/2019.17096.

10. Hsu, L.T. What are the roles of artificial intelligence and machine learning in GNSS positioning ? *Inside GNSS* **2020**, pp. 1–8.
11. Sharaf, R.; Noureldin, A.; Osman, A.; El-Sheimy, N. Online INS/GPS Integration with a Radial Basis Function Neural Network. *IEEE Aerospace and Electronic Systems Magazine* **2005**, *20*, 8–14. doi:10.1109/MAES.2005.1412121.
12. Semeniuk, L.; Noureldin, A. Bridging GPS outages using neural network estimates of INS position and velocity errors. *Measurement Science and Technology* **2006**, *17*, 2783–2798. doi:10.1088/0957-0233/17/10/033.
13. Sharaf, R.; Noureldin, A. Sensor Integration for Satellite-Based Vehicular Navigation Using Neural Networks. *IEEE Transactions on Neural Networks* **2007**, *18*, 589–594. doi:10.1109/TNN.2006.890811.
14. Ragab, M.M.; Ragab, H.; Givigi, S.; Noureldin, A. Performance evaluation of neural-network-based integration of vision and motion sensors for vehicular navigation. Autonomous Systems: Sensors, Processing, and Security for Vehicles and Infrastructure 2019; Dudzik, M.C.; Ricklin, J.C., Eds. International Society for Optics and Photonics, SPIE, 2019, Vol. 11009, pp. 140 – 151. doi:10.1117/12.2521694.
15. Jaradat, M.A.; Abdel-Hafez, M.F.; Saadeddin, K.; Jarrah, M.A. Intelligent fault detection and fusion for INS/GPS navigation system. 2013 9th International Symposium on Mechatronics and its Applications (ISMA). IEEE, 2013, pp. 1–5. doi:10.1109/ISMA.2013.6547398.
16. Du, S.; Gan, X.; Zhang, R.; Zhou, Z. The Integration of Rotary MEMS INS and GNSS with Artificial Neural Networks. *Mathematical Problems in Engineering* **2021**, *2021*, 1–10. doi:10.1155/2021/6669682.
17. Al Bitar, N.; Gavrilov, A. A new method for compensating the errors of integrated navigation systems using artificial neural networks. *Measurement* **2021**, *168*, 108391. doi:10.1016/j.measurement.2020.108391.
18. Tamazin, M.; Korenberg, M.J.; Elghamrawy, H.; Noureldin, A. GPS Swept Anti-Jamming Technique Based on Fast Orthogonal Search (FOS). *Sensors* **2021**, *21*, 3706. doi:10.3390/s21113706.
19. Iqbal, U.; Abosekeen, A.; Georgy, J.; Umar, A.; Noureldin, A.; Korenberg, M.J. Implementation of Parallel Cascade Identification at Various Phases for Integrated Navigation System. *Future Internet* **2021**, *13*, 191. doi:10.3390/fi13080191.
20. Sánchez Morales, E.; Dauth, J.; Huber, B.; García Higuera, A.; Botsch, M. High Precision Outdoor and Indoor Reference State Estimation for Testing Autonomous Vehicles. *Sensors* **2021**, *21*, 1131. doi:10.3390/s21041131.
21. Semanjski, S.; Semanjski, I.; De Wilde, W.; Muls, A. Use of Supervised Machine Learning for GNSS Signal Spoofing Detection with Validation on Real-World Meaconing and Spoofing Data—Part I. *Sensors* **2020**, *20*, 1171. doi:10.3390/s20041171.
22. Sabzevari, D.; Chatraei, A. INS/GPS Sensor Fusion based on Adaptive Fuzzy EKF with Sensitivity to Disturbances. *IET Radar, Sonar & Navigation* **2021**, *15*, 1535–1549. doi:10.1049/rsn2.12144.
23. Cao, H.; Wei, W.; Liu, L.; Ma, T.; Zhang, Z.; Zhang, W.; Shen, C.; Duan, X. A Temperature Compensation Approach for Dual-Mass MEMS Gyroscope Based on PE-LCD and ANFIS. *IEEE Access* **2021**, *9*, 95180–95193. doi:10.1109/ACCESS.2021.3094120.
24. Duan, Y.; Li, H.; Wu, S.; Zhang, K. INS Error Estimation Based on an ANFIS and Its Application in Complex and Covert Surroundings. *ISPRS International Journal of Geo-Information* **2021**, *10*, 388. doi:10.3390/ijgi10060388.
25. Aouf, A.; Boussaid, L.; Sakly, A. TLBO-Based Adaptive Neurofuzzy Controller for Mobile Robot Navigation in a Strange Environment. *Computational Intelligence and Neuroscience* **2018**, *2018*, 1–8. doi:10.1155/2018/3145436.
26. Zhang, Y. A Fusion Methodology to Bridge GPS Outages for INS/GPS Integrated Navigation System. *IEEE Access* **2019**, *7*, 61296–61306. doi:10.1109/ACCESS.2019.2911025.
27. Yue, S.; Cong, L.; Qin, H.; Li, B.; Yao, J. A Robust Fusion Methodology for MEMS-Based Land Vehicle Navigation in GNSS-Challenged Environments. *IEEE Access* **2020**, *8*, 44087–44099. doi:10.1109/ACCESS.2020.2977474.
28. Li, Y.; Chen, R.; Niu, X.; Zhuang, Y.; Gao, Z.; Hu, X.; El-Sheimy, N. Inertial Sensing Meets Machine Learning: Opportunity or Challenge? *IEEE Transactions on Intelligent Transportation Systems* **2021**, pp. 1–17. doi:10.1109/TITS.2021.3097385.
29. Groves, P.D. *Principles of GNSS, inertial, and multisensor integrated navigation systems*, 2nd ed.; Artech House: Boston, London, 2008; p. 505.
30. Savage, P.G. Strapdown Inertial Navigation Integration Algorithm Design Part 2: Velocity and Position Algorithms. *Journal of Guidance, Control, and Dynamics* **1998**, *21*, 208–221. doi:10.2514/2.4242.
31. Abosekeen, A. Multi-Sensor Integration and Fusion in Navigation Systems. Msc., Military Technical College, 2012. doi:10.13140/RG.2.1.1967.5603.
32. Abosekeen, A.; Noureldin, A.; Korenberg, M.J. Improving the RISS/GNSS Land-Vehicles Integrated Navigation System Using Magnetic Azimuth Updates. *IEEE Transactions on Intelligent Transportation Systems* **2020**, *21*, 1250–1263. doi:10.1109/TITS.2019.2905871.
33. Diebel, J. Representing attitude: Euler angles, unit quaternions, and rotation vectors. *Matrix* **2006**, *58*, 1–35.
34. Zhang, L.; Liu, J.; Lai, J.; Xiong, Z. Performance analysis of adaptive neuro fuzzy inference system control for mems navigation system. *Mathematical Problems in Engineering* **2014**, *2014*, 1–7. doi:10.1155/2014/961067.
35. Al-Hmouz, A.; Shen, J.; Al-Hmouz, R.; Yan, J. Modeling and Simulation of an Adaptive Neuro-Fuzzy Inference System (ANFIS) for Mobile Learning. *IEEE Transactions on Learning Technologies* **2012**, *5*, 226–237. doi:10.1109/TLT.2011.36.
36. Bhattacharyya, S.; Dutta, P. Fuzzy Logic: Concepts, System Design, and Applications to Industrial Informatics. In *Handbook of Research on Industrial Informatics and Manufacturing Intelligence: Innovations and Solutions*; Khan, M.A.; Ansari, A.Q., Eds.; IGI Global: Hershey, PA, 2012; chapter 3, pp. 33–71. doi:10.4018/978-1-4666-0294-6.ch003.
37. Sivakumar, R.; Sahana, C.; Savitha, P. Design of ANFIS based Estimation and Control for MIMO Systems. *International Journal of Engineering ...* **2012**, *2*, 2803–2809.

38. Erdem, H. Application of Neuro-Fuzzy Controller for Sumo Robot control. *Expert Systems with Applications* **2011**, *38*, 9752–9760. doi:10.1016/j.eswa.2011.02.024.
39. Jang, J.S. ANFIS: adaptive-network-based fuzzy inference system. *IEEE Transactions on Systems, Man, and Cybernetics* **1993**, *23*, 665–685. doi:10.1109/21.256541.